Journal of
Marine Science and Engineering

MDPI

Article

Borehole Instability in Decomposed Granite Seabed for Rock-Socketed Monopiles during "Drive-Drill-Drive" Construction Process: A Case Study

Bo Sun [1], Qi Zhang [1,*], Wenxuan Zhu [1], Jian Leng [2] and Guanlin Ye [1]

[1] State Key Laboratory of Ocean Engineering, Department of Civil Engineering, Shanghai Jiao Tong University, Shanghai 200240, China; bo.sun@sjtu.edu.cn (B.S.); zhuwx1992@sjtu.edu.cn (W.Z.); ygl@situ.edu.cn (G.Y.)
[2] CCCC Third Harbor Engineering Co., Ltd., Shanghai 200032, China; keepwalkinglj@163.com
* Correspondence: zhangqi33@sjtu.edu.cn

Abstract: Monopiles are commonly used in the construction of offshore wind turbines. However, implementing drive-drill-drive construction techniques in decomposed granite seabed may lead to borehole instability during the window period between drilling and pile driving, resulting in significant project losses. This study provides a comprehensive understanding and approach to address the causes of borehole instability in rock-socketed monopiles in decomposed granite seabed. Using the Pinghai Bay offshore wind farm project in Fujian, China as an example, the details of drive-drill-drive and reverse-circulation drilling techniques employed in monopile construction were introduced. An improved sampling method was utilized to obtain decomposed granite samples, and a series of in situ and laboratory tests were conducted to analyze the physical and mechanical properties of marine-decomposed granite. By examining three cases of monopile construction, the factors contributing to borehole instability during rock-socketed monopile construction in decomposed granite seabed were identified, and corresponding recommendations were proposed. The results indicated that construction technology and unfavorable geological characteristics of decomposed granite are the primary causes of borehole instability. Collapses occurred mainly in highly and moderately decomposed granite layers. Employing smaller boreholes can reduce the likelihood and impact of borehole instability.

Keywords: borehole instability; decomposed granite; rock-socketed monopile; field case

check for updates

Citation: Sun, B.; Zhang, Q.; Zhu, W.; Leng, J.; Ye, G. Borehole Instability in Decomposed Granite Seabed for Rock-Socketed Monopiles during "Drive-Drill-Drive" Construction Process: A Case Study. *J. Mar. Sci. Eng.* **2023**, *11*, 990. https://doi.org/10.3390/jmse11050990

Academic Editor: M. Dolores Esteban

Received: 19 March 2023
Revised: 20 April 2023
Accepted: 6 May 2023
Published: 6 May 2023

1. Introduction

Offshore wind power is an important contributor to mitigating the effects of climate change and reducing the global carbon footprint. The construction of offshore wind turbines has seen a significant increase in recent years to meet the growing demand for renewable energy [1]. However, offshore wind turbine construction presents a unique set of challenges, one of them being the elevated cost compared to onshore wind turbine construction [2]. Among the contributing factors to the elevated cost of offshore wind turbine construction are the design and installation of the foundation account for a substantial portion, potentially reaching 20–30% [3].

The foundations for offshore wind turbines can take various forms, such as gravity, monopiles, tripods, jackets, and suction bucket foundations [4]. Among these, monopiles have become a popular choice for offshore wind power due to their simplicity and cost-effectiveness [5–7]. Despite their popularity, monopile construction in certain geological formations can pose problems that result in increased foundation installation costs. In southeastern China, granites with varying degrees of weathering are widely present on the seabed [8,9]. The construction of monopiles in this area requires passing through decomposed granite, which led to frequent incidents of borehole instability and pile running during construction. These incidents have a significant impact on the safety and economics of offshore wind turbine construction.

Borehole instability is a major concern in drilling operations and has been studied in different formations. In anisotropic rocks, when the borehole is perpendicular to the bedding plane, the influence of the bedding plane on the wellbore instability is negligible, while the borehole instability is prone to occur when the borehole is oriented along the bedding plane [10]. Borehole instabilities in shale involve multiple mechanisms, including pore pressure diffusion, plasticity, anisotropy, capillary effects, permeability, and physicochemical changes [11]. In sandstones with moderate to high porosity and rich in quartz, borehole instabilities result in the formation of elongated, slender fractures that extend to substantial distances and are oriented perpendicular to the far-field principal compressive stress [12]. The failure mode of sandy soil in the borehole was found to be primarily governed by shear failure [13]. Extensive model borehole tests showed that in clay formations, over-consolidation can greatly improve the stability of the borehole, and for normally consolidated clay, the hole wall becomes unstable when the volume change exceeds 5% [14]. However, borehole stability performance in decomposed granite seabed is still not fully understood and is an area of scarce research.

To fully understand the causes of borehole instability of rock-socketed monopile in decomposed granite seabed, a series of in situ and laboratory tests were carried out to reveal the engineering geological characteristics of the decomposed granite in the southeastern coastal region of China. Combining three cases of monopile construction, the reasons for borehole instability during the construction process of rock-socketed monopiles in the decomposed granite seabed were clarified, and corresponding countermeasures were proposed. The results of this study can provide a reference for the construction of offshore wind power projects in similar geological formations.

2. Background

2.1. Project Information

As part of the Pinghai Bay Offshore Wind Power Project, the offshore wind farm is located near Luci Island in the southeastern region of China, as shown in Figure 1. The site has been designated for the installation of 50 wind turbines, each with a capacity of 5 MW, yielding a total installed capacity of 250 MW. The water depth within the site varied between 10~20 m, with the closest distance to the coastline estimated at approximately 6.0 km. The primary foundation forms utilized for the wind turbines are steel tube monopiles, group pile foundations, and suction bucket foundations, with an initial plan to utilize monopiles for 28 wind turbines. However, due to construction challenges such as borehole collapse and pile running, the number of wind turbines employing monopiles was reduced to 16.

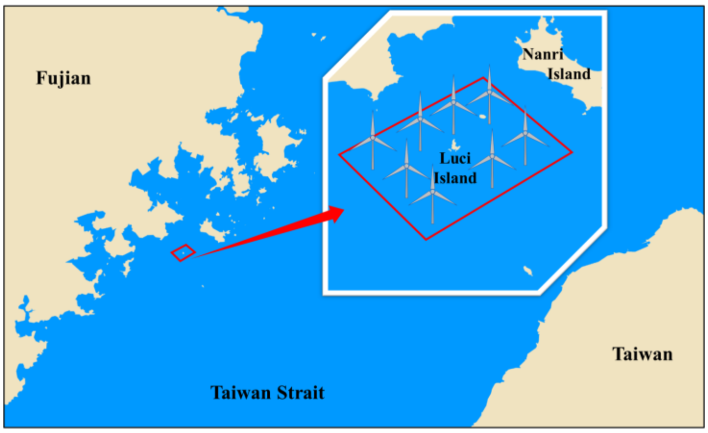

Figure 1. The location of the offshore wind farm.

The geological characteristics of this area, identified by drilling surveys conducted in the study area, are characterized by a soft top layer and a hard bottom layer. The overlying soil is the result of extensive weathering of offshore rocks and sediments, while the bottom is primarily composed of moderately decomposed granite (MDG) to slightly decomposed granite (SDG) with a relatively intact rock mass and high hardness. Between the two layers are completely decomposed granite (CDG) and highly decomposed granite (HDG), which are sensitive to disturbance and tend to soften when exposed to water.

The construction of offshore wind power foundations is significantly influenced by the marine environment. Typically, construction activities are carried out for 3~4 consecutive days under ideal weather conditions. However, the area is frequently affected by unfavorable weather conditions from October to March of the subsequent year, and the continuity of construction is significantly affected. The optimal construction period occurs from April to September annually, although this timeframe is subject to typhoon disruptions. Data obtained from historical records of the construction site and local meteorological stations show that the construction site is typically impacted by 5~6 typhoons each year, with each typhoon resulting in 3~7 days of suspension. The restricted effective construction time necessitates stringent demands on the construction of offshore wind power foundations and the installation of offshore wind turbines.

2.2. Construction Technology

The construction of monopiles typically employs pile-driving construction technology, which involves driving the pile to the required depth using a hydraulic hammer. During the construction process in the area of Pinghai Bay, the monopile could easily penetrate the surface sedimentary soil layers. However, the pile-driving method is no longer effective due to the high soil shear strength when reaching the decomposed granite stratum. To address this issue, the construction method was altered to "drive-drill-drive" construction technology [15], as shown in Figure 2. The process is as follows:

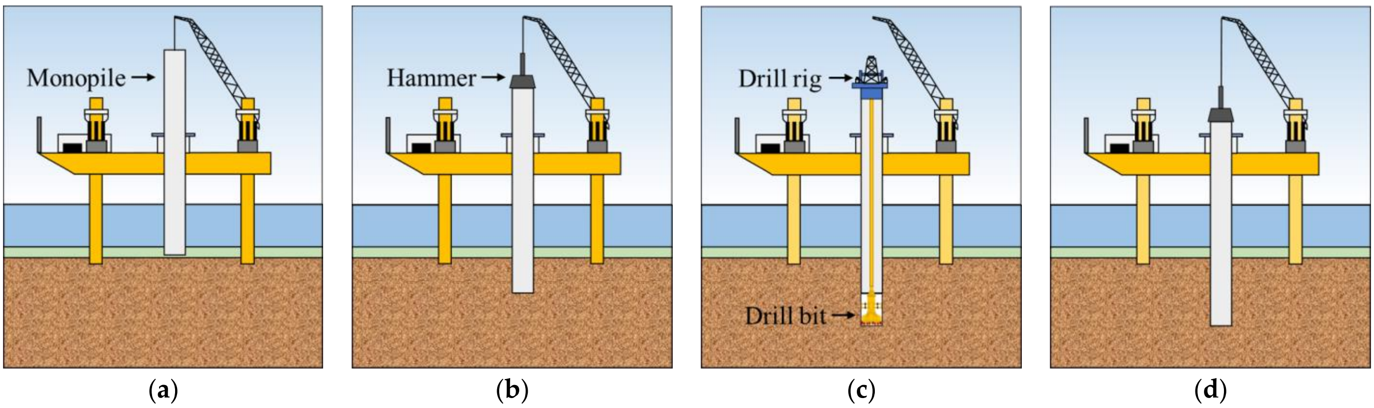

Figure 2. Construction process of monopile: (**a**) locating monopile on the seabed, (**b**) pile driving, (**c**) drilling hole, and (**d**) pile driving.

The monopile is first positioned into the cage mouth using a crane and then pressed down with a hydraulic hammer. When the monopile reaches a certain depth and encounters harder formation, it is difficult to move downward. At this stage, a drilling rig is utilized to hollow out the soil in the monopile, and drilling is continued for a set distance to reduce the resistance for driving the monopile. After the drilling rig is drilled to the desired depth, the piling equipment is replaced to further drive the monopile into a deeper formation. This process of drilling and pile driving is repeated until the pile foundation reaches the design depth. The on-site construction of pile driving and drilling rig hoisting is shown in Figure 3.

Figure 3. The on-site construction of: (**a**) monopile driving and (**b**) drilling rig hoisting.

To complete the installation of the offshore wind turbine foundations within the limited construction window, the highly efficient and rapid gas-lift reverse-circulation construction technology was employed during the drilling phase, as illustrated in Figure 4. The reverse-circulation construction process entails directing compressed air into the drill bit through the annular space of the double wall drill pipe, causing the compressed air to mix with seawater and the drill cuttings generated during drilling to form a low-density gas–liquid mixture [16]. The resulting difference in liquid density between the inside and outside of the pipe drives the cuttings in the drill hole to be transported from the inner pipe to the surface via water flow, creating a cyclical reaction. This process enables a significant amount of drill cuttings to be efficiently discharged in a short period, thereby significantly increasing the construction speed.

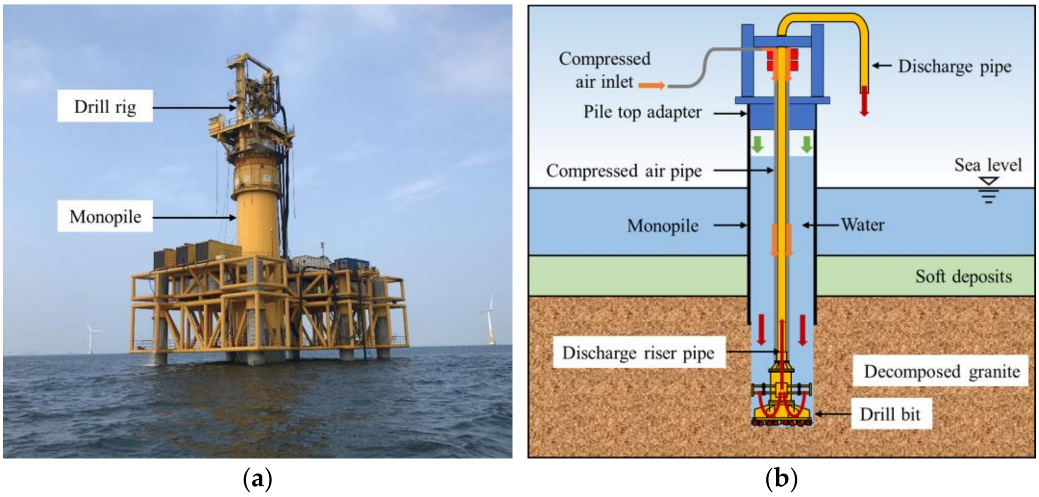

Figure 4. Reverse-circulation drilling: (**a**) photo of drilling rig and (**b**) schematic diagram of drilling.

2.3. Borehole Instability

During the construction of the monopile at the Pinghai Bay offshore wind farm, borehole instability problems occurred several times, which occurred during the transitional period between drilling and pile driving, leading to issues such as pile running and deviation from the desired pile verticality. These problems resulted in prolonged construction periods and increased costs.

Borehole instability often occurs during the window between the drilling and pile driving processes, which required the transportation and replacement of large-scale construction machinery by offshore engineering vessels. This transition period, which often lasted several days, caused the soil near the exposed hole wall to collapse and fall, triggering a cascading collapse of the hole wall, as shown in Figure 5. During the construction process of the monopiles for the 16 wind turbines at the wind farm, varying degrees of collapse occurred. Among them, pile running occurred during the construction of three monopiles due to the large range of hole wall collapse. In the construction process of the remaining monopiles, the bottom elevation of the holes increased by 0.5 to 5 m compared to the pre-collapse level due to the hole wall collapse.

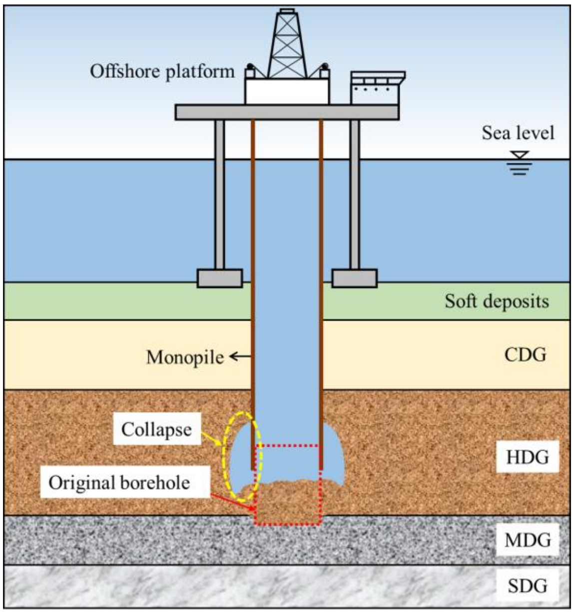

Figure 5. Schematic diagram of hole collapse after drilling.

2.4. Typical Borehole Collapse Cases

2.4.1. Case 1

The geological conditions and collapse situation of Case 1 are shown in Figure 6. The water depth is 15.45 m, and the overlying layer is 16.4 m thick, primarily consisting of silt-fine sand and medium-fine sand. The lower part of the surface seabed sediments is composed of CDG, HDG, and MDG. The CDG layer has a thickness of 3.6 m, the HDG has a thickness of 19.5 m, and the MDG is located below it. At first, the monopile was driven to a depth of 33.25 m, with the bottom of the monopile located in the HDG layer, followed by drilling operations. After five days of drilling, the depth reached 6.25 m below the monopile tip, with the exposed rock thickness being 6.15 m in the HDG layer and 0.1 m in the MDG layer. Subsequently, the plan was to replace the driving equipment for further pile driving, but the equipment arrived 12 days after the completion of drilling, and a collapse problem occurred in the meantime. The elevation of the pile bottom had increased by 5 m due to the borehole collapse, which mainly occurred in the HDG layer.

2.4.2. Case 2

The geological conditions and collapse situation of Case 2 are presented in Figure 7. The overlying layer is 6.8 m thick and consists mainly of silt-fine sand. The lower part of the surface seabed sediments consists of HDG, and there is no CDG stratum at this turbine location. The HDG stratum has a thickness of 12.75 m, and the MDG stratum below it has a thickness of 13.7 m. After the completion of monopile driving, the monopile entered the strata at a depth of 26.85 m, followed by drilling operations. The drilling depth reached 8.4 m below the monopile tip, with 2.1 m of the exposed rock being in the SDG stratum. Subsequently, the plan was to replace the piling equipment for further piling, with the equipment arriving 10 days after the completion of the drilling. However, it was discovered that a collapse had occurred. Upon testing, it was found that the elevation of the monopile bottom had increased by 4.2 m due to the collapse, which mainly occurred in the MDG stratum.

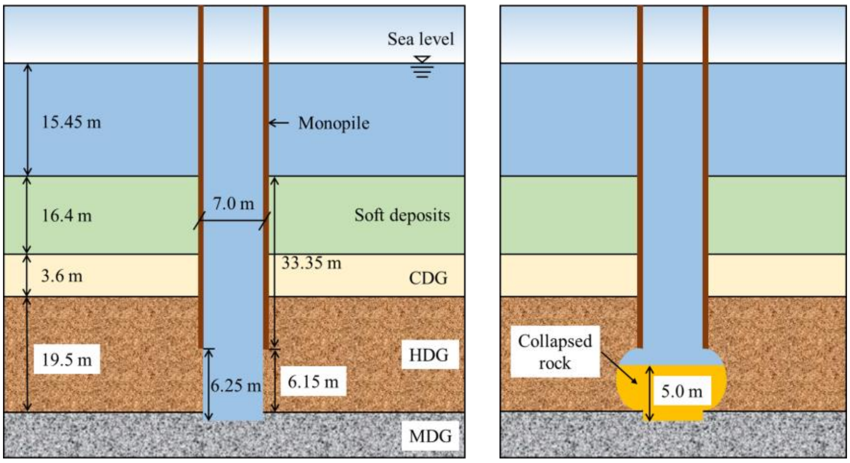

(**a**) (**b**)

Figure 6. Borehole instability of Case 1: (**a**) original borehole and (**b**) borehole after the collapse.

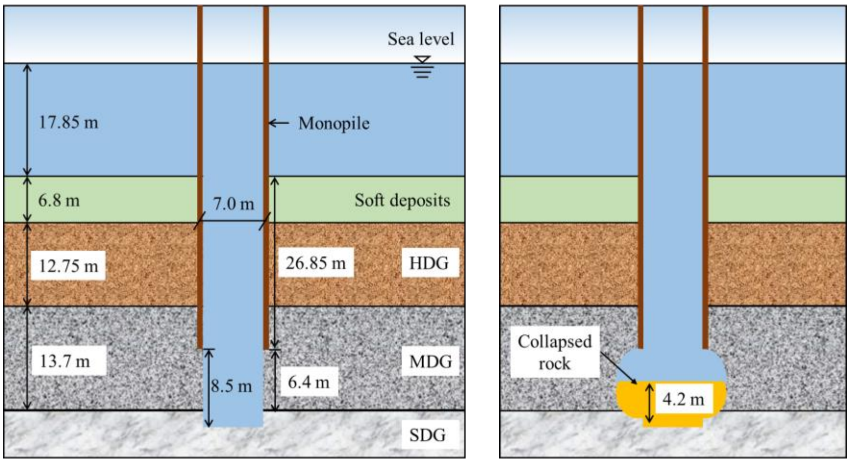

(**a**) (**b**)

Figure 7. Borehole instability of Case 2: (**a**) original borehole and (**b**) borehole after the collapse.

2.4.3. Case 3

The geological conditions and collapse situation in Case 3 are depicted in Figure 8. The overlying layer is 24.6 m thick, consisting mainly of silt-fine sand and powdery clay. The lower part of the surface seabed sediments comprises HDG, with the CDG stratum missing at this location, similar to Case 2. The HDG stratum has a thickness of 7.9 m, with the MDG stratum below it. The monopile had a depth of 33.2 m in the strata, with the bottom of the monopile located in the MDG stratum, followed by drilling operations. After 10 days of drilling, the drilling depth reached 4.9 m below the monopile tip, with all exposed rock being in the MDG stratum. Subsequently, the plan was to replace the piling equipment for further piling, with the equipment arriving 12 days after the completion of the drilling. However, a collapse problem occurred, and it was found that the elevation of the monopile bottom had increased by 4.8 m due to the collapse, which mainly occurred in the MDG stratum.

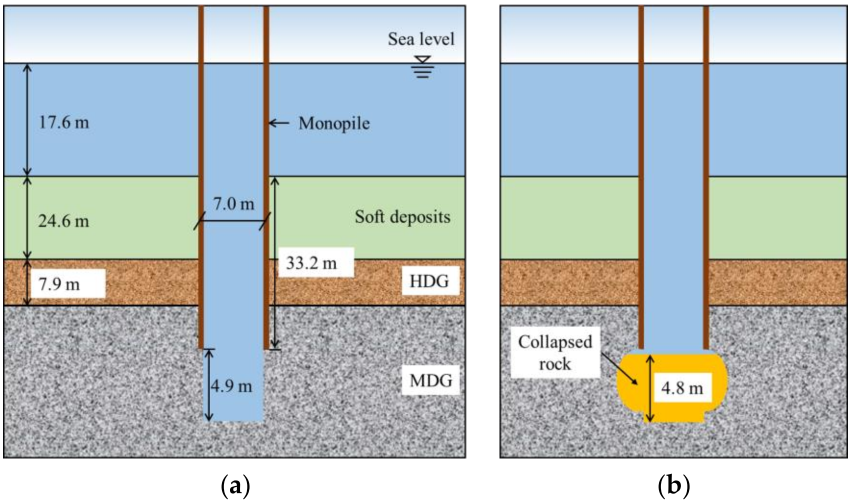

Figure 8. Borehole instability of Case 3: (**a**) original borehole and (**b**) borehole after the collapse.

3. Methodology

Since the borehole instability of rock-socketed monopile in decomposed granite seabed is closely related to the physical and mechanical properties of the granite, a series of in situ and laboratory tests were first carried out.

3.1. Sampling Method

Due to the poor mechanical properties of the soil, especially for the completely decomposed granite (CDG) and highly decomposed granite (HDG), a less disturbed field sampling method was adopted. The sampling process is depicted in Figure 9. Firstly, the casing was lowered to the seabed surface and the drilling rig was secured on the platform. The soil sampler was then installed on the drill pipe and lowered from within the casing to the seabed surface. The drilling rig rotated the drill pipe and extracts soil samples while a slurry pit and a pump were employed on the platform to circulate drilling fluid in the borehole and remove drilling debris.

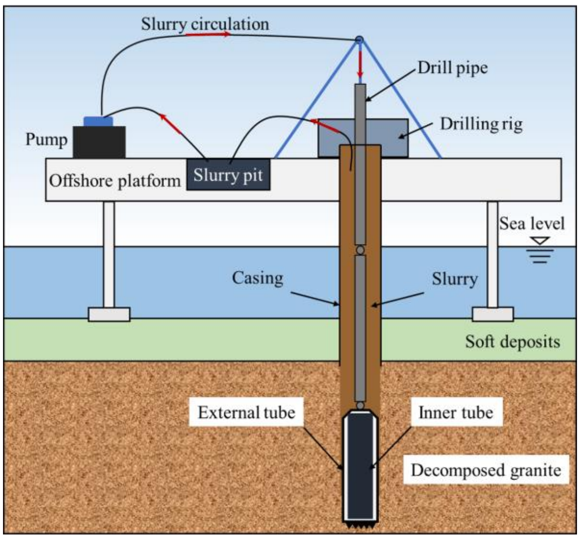

Figure 9. Schematic diagram of the soil sampling method.

As shown in Figure 10, the soil sampler utilized was a double-tube rotary sampler, with the outer tube rotating during the soil retrieval process, while the inner core tube remained stationary [17]. This method reduces the impact of vibration on the soil samples during the sampling process, minimizes scouring of the soil samples by the drilling liquid, and effectively reduces the disturbance to soil samples [18]. To enhance the performance of the slurry and ensure the quality of the retrieved soil, a certain amount of biopolymer was added to the drilling fluid. Biopolymer is a natural, organic high molecular polymer that comes in the form of a light red powder and is soluble in water [19]. The drilling fluid prepared with biopolymer exhibits improved viscoelasticity, lubricity, and rheology compared to the traditional slurry, effectively reducing the mechanical vibration of the drill pipe, protecting the core and hole wall, and being non-toxic and biodegradable. To gain a comprehensive understanding of the soil properties in the sea region of the offshore wind farm, a total of 22 sampling locations within the sea region were drilled, and samples were collected.

Figure 10. Double-tube rotary sampler sampling of marine-decomposed granite: (**a**) drilling rig, (**b**) double-tube rotary sampler, (**c**) biopolymer, and (**d**) sample.

3.2. In Situ Tests

In this research, various techniques were utilized for geological surveying, including the standard penetration test (SPT), heavy cone dynamic probing test (DPT), shear wave velocity tests, and resistivity tests. Standard penetration tests were carried out on the overlying soil layers such as silt-fine sand, powdery clay, and the CDG and HDG soil layers. An automatic hammer device with a hammer weight of 63.5 kg and a fall distance of 7 cm was used for the test. During the test, after pre-drilling 15 cm, the probe was kept vertical, and the hammer was struck at a uniform speed. The number of standard penetrations for each 10 cm and the cumulative penetration of 30 cm were recorded as one test point. The penetration depth at the 50th blow was recorded when the number of standard penetrations reached 50 within 30 cm. Standard penetration tests were conducted on each layer inside the borehole with a spacing of 2~3 m within a depth of 0~20 m.

In the MDG stratum, heavy dynamic probing tests were conducted using an automatic disengagement free-fall hammer for penetration, with continuous penetration required, and the number of blows were recorded for every 10 cm. Heavy dynamic probing tests were carried out every 2~3 m, with a continuous penetration of no less than 1 m per layer in the same geological unit.

In this study, shear wave velocity tests were conducted on each soil layer using a suspended wave velocity logger. The equipment included a host machine, an in-well suspended probe, and connecting cables, such as signal cables and trigger cables. The in-well suspended probe was composed of a fully sealed electromagnetic excitation source, two independent fully sealed detectors, and high-strength connection hoses, with a distance of 1 m between the two receiving detectors. The shear wave testing was conducted after the completion of drilling and before the stratum shrinkage, with a test point spacing of 1 m in the uncased borehole. Electrical resistivity testing was also conducted after sampling, with an electrode spacing of 0.1 m and 0.95 m.

3.3. Laboratory Tests

After the completion of the sampling work, samples were promptly sealed with wax, labeled, placed in shockproof boxes, and sent to the laboratory. To ensure the quality of undisturbed samples, efforts were made to minimize human disturbances during the packaging, transportation, storage, protection, and delivery of soil samples. Based on ASTM D2487 (2011) standard [20], the laboratory conducted tests to determine the basic physical indicators of rock and soil, including natural density (ρ_n), dry density (ρ_d), void ratio (e), water content (ω), specific gravity of solid particles (G_s), and permeability coefficient (k). Mechanical indicators of rock and soil, including compression coefficient $a_{v0.1\sim0.2}$ (the slope of the tangent of the e-p compression curve when the pressure p is between 0.1 and 0.2 MPa), compression modulus $E_{s1\sim2}$ (calculated when the additional pressure p equals 1 and 2 MPa), and elastic modulus (E_e), were also obtained. The cohesive strength (c) and internal friction angle (φ) of the CDG and HDG were determined through direct simple shear tests, while the point load strength index (I_s) of the MDG was obtained through point load tests. The uniaxial compressive strength (R) of the MDG and SDG was determined through a uniaxial compression test.

CDG and HDG exhibit disintegration properties when immersed in water, which can accelerate the collapse of borehole walls. To investigate this characteristic, disintegration tests were performed by immersing samples in a saline solution.

4. Results and Discussion

4.1. Physical and Mechanical Properties of Decomposed Granite

Typical samples of four types of weathered granite are displayed in Figure 11. Table 1 summarizes the typical characteristics of four types of weathered granite classified according to the degree of weathering and physical properties, and the weathering classification system for granite and volcanic rocks in Hong Kong [21,22] is referenced. Based on data from 22 drilling sites in Pinghai Bay and laboratory tests, Table 2 summarizes the physical properties of the four types of weathered granite, including shear wave velocity (V_s), resistivity (ρ), and the standard penetration test number (N). The sample morphology in Figure 11, combined with the qualitative indicators of the samples in Table 2 and the general description of the sample properties in Table 1, can be used to conveniently classify weathered granite according to the degree of weathering in engineering.

Table 1. Classification of differently decomposed granite.

Type	Grade	General Characteristics	Typical Characteristics
CDG	V	Gray-yellow with brown yellow Destroyed completely, soil like	High content of clay minerals Can be crumbled by hand
HDG	IV	Gray-white with black	Mainly quartz and feldspar
		Original rock texture preserved, sandy soil like	Can be broken by hand
MDG	III	Brown yellow	Part of feldspar is weathered
		Clear structure of parent rocks, clastic blocks	Not easily broken by hand, easily broken by hammer
SDG	II	Gray-white with black	Mainly quartz, feldspar, and mica
		Distinct structure of parent rocks, column-like	Cannot usually be broken by hand, not easily broken by hammer

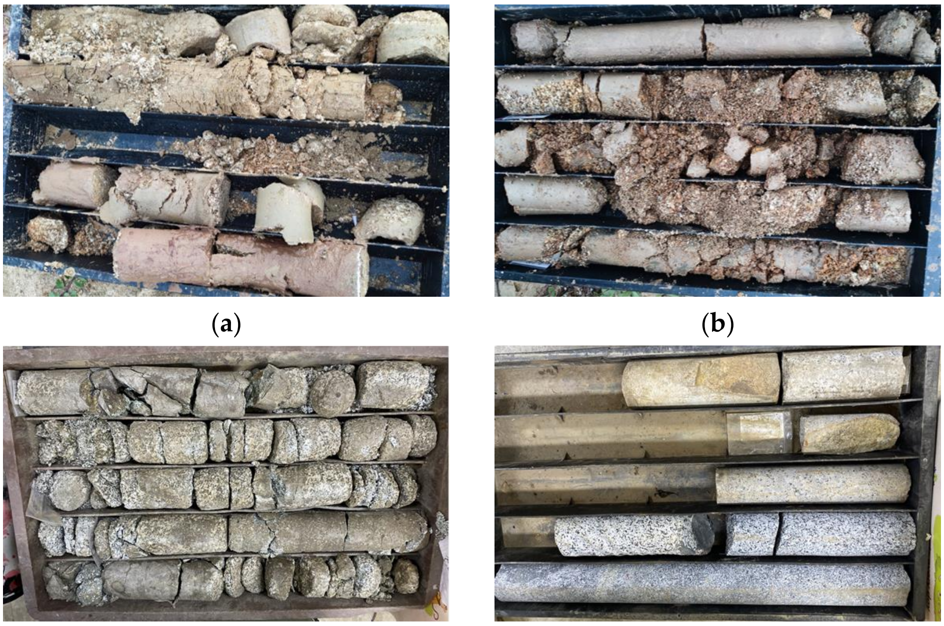

(**a**) (**b**) (**c**) (**d**)

Figure 11. Typical images of different decomposed granite: (**a**) CDG, (**b**) HDG, (**c**) MDG, and (**d**) SDG.

Table 2. Main physical and mechanical properties of decomposed granite.

Parameter	CDG	HDG	MDG	SDG
$\rho_n/(\text{g/cm}^3)$	1.83~2.04	1.87~2.21	/	/
$\rho_d/(\text{g/cm}^3)$	1.50~1.73	1.46~1.92	2.68~2.72	2.62~2.81
e	0.552~0.814	0.397~0.850	/	/
$\omega/\%$	17.7~29.9	14.3~30.6	/	/
G_s	2.69~2.72	2.68~2.72	/	/
$a_{v0.1\sim0.2}/\text{MPa}^{-1}$	0.30~0.54	0.23~0.28	/	/
$E_{s1\sim2}/\text{MPa}$	3.35~5.49	5.53~11.61	/	/
E_e/GPa	/	/	/	16.8~51.9
c/kPa	21.3~25.3	18.3~23.4	205.9~6900	/
$\varphi/^\circ$	27.4~28.8	28.4~35.2	34.9~52.4	/
I_s/MPa	/	/	0.33~0.68	/
R/MPa	/	/	5.38~18.20	30.63~107.20
$k/(10^{-6}\ \text{cm/s})$	58.2~87.5	61.2~426.0	/	/
$V_s/(\text{m/s})$	311~346	316~495	447~681	610~936
$\rho/(\Omega{\cdot}\text{m})$	1.46~1.91	2.18~11.36	10.73~44.26	23.66~152.55
N	33~47	55~67	/	/

Overall, both CDG and HDG have undergone significant weathering processes, resulting in poor engineering geological properties similar to residual soil. Some physical indicators of CDG and HDG, such as natural density (ρ_n), dry density (ρ_d), void ratio (e), water content (ω), specific gravity of solid particles (G_s), and permeability coefficient (k), are comparable in magnitude and overlap. The compression coefficient ($a_{v0.1\sim0.2}$) and the compression modulus ($E_{s1\sim2}$) of CDG are significantly smaller than those of HDG, indicating that CDG is more compressible. The strengths of CDG and HDG are similar and relatively low, with cohesion (c) around 20 kPa, an internal friction angle (φ) of approximately 28° for CDG, and approximately 32° for HDG. There are noticeable differences in the field test indicators of CDG and HDG, manifested as higher shear wave velocity (V_s), resistivity (ρ), and standard penetration test number (N) for CDG than HDG.

In contrast to CDM and HDG, MDG exhibits overall characteristics of fragmented rock mass. MDG rock blocks retain part of the original rock strength, such as block cohesion (c) and point load strength (I_s) reaching several thousand kPa, and uniaxial compressive strength (R) around 10 MPa. The shear wave velocity (V_s) and resistivity (ρ) of MDG are significantly higher than those of CDG and HDG. Although the strength of individual MDG rock blocks is substantial, the structure of the MDG rock mass is extremely fragmented, with an average spacing of structural surfaces less than 0.4 m, making the rock mass prone to failure along these structural surfaces.

Among the four rock types, SDG exhibits the lowest degree of weathering, with core strength closer to fresh rock and the highest uniaxial compressive strength (R) reaching approximately 100 MPa. Additionally, the rock mass structure of SDG is relatively intact, with structural surface spacing greater than 1 m. Moreover, the shear wave velocity (V_s) and resistivity (ρ) of SDG are higher than those of MDG.

4.2. Disintergration Properties of Decomposed Granite

The typical images of the samples during disintegration are shown in Figure 12, where t represents the immersion time and R_d represents the percentage of disintegration of the sample. The disintegration process of CDG due to water immersion shows a gradual disintegration from the outside to the inside. Surface particles detach continuously from the sample, falling to the bottom of the container. The sample disintegrates rapidly, and a significant quantity of soil particles enter the solution, forming a suspension in a short time, leading to complete disintegration. During the disintegration process of CDG, multiple cracks occur, causing small samples to disintegrate quickly and fall to the bottom of the screen, while larger samples remain relatively stable for a short time before additional cracking occurs.

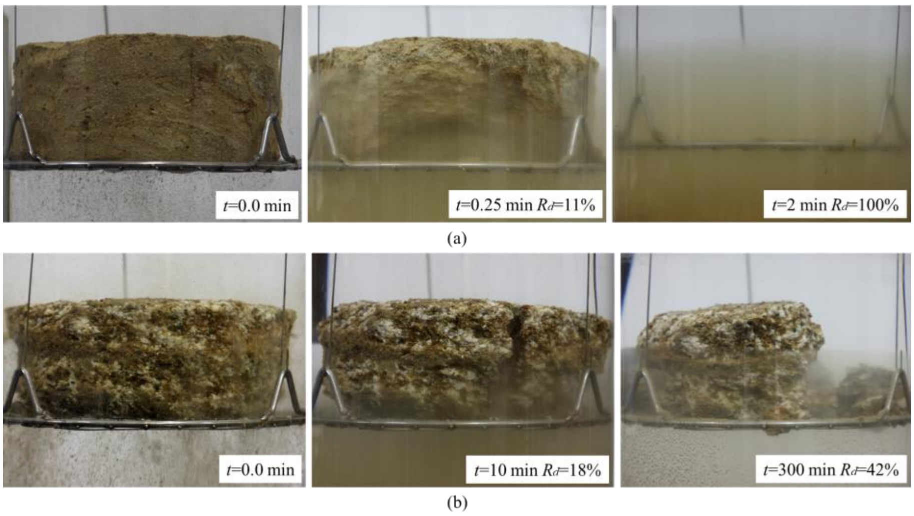

Figure 12. Typical images of samples during disintegration: (**a**) CDG with a buried depth of 3.5 m and (**b**) HDG with a buried depth of 9.6 m.

The results of the disintegration tests are presented in Figure 13. The disintegration rate of CDG was relatively fast, and it completely disintegrated in approximately 2 min. The disintegration process occurred gradually from the outside to the inside, resulting in a smooth disintegration curve. In contrast, HDG had a slower disintegration rate and demonstrated resistance to disintegration. During the process, multiple cracks were observed, and the disintegration curve showed a step-like increase. The disintegration rate and ratio varied based on the depth of burial, with the sample buried at a depth of 6.5 m taking approximately 10 min to reach a stable disintegration state with a final disintegration ratio (R_d) of approximately 80%. The sample buried at 9.6 m took around 2 h to reach a stable disintegration state with R_d of 42%, while the sample buried at a depth of 12.8 m showed only a small amount of disintegration after 2 to 3 h and took 10 h to reach a stable state, with R_d of 16%.

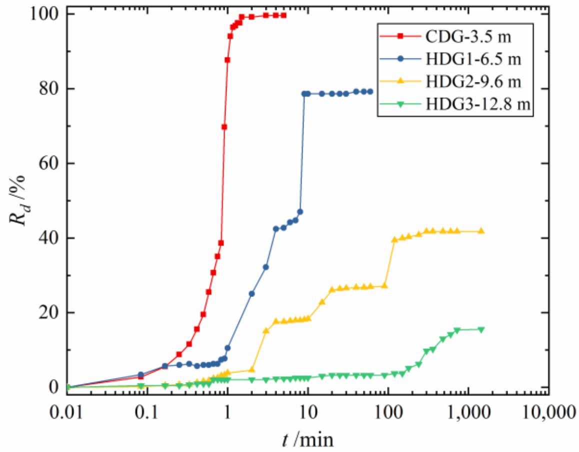

Figure 13. Disintegration curves of granite with different weathering degrees.

4.3. Causes for Borehole Instability

During the monopile construction, it was observed that hole wall collapse was primarily an issue in the HDG or MDG stratum. This was due to the high resistance encountered during monopile driving in this layer, which requires switching from piling to drilling methods. In contrast, the sedimentary layer on the seabed surface and the CDG formation has low soil strength, allowing the monopile to penetrate without the need for drilling equipment. However, after drilling is completed, the HDG and CDG tend to collapse before the next piling. When entering the SDG, the switch between piling and drilling is also required, but the low degree of weathering of SDG results in the stability of the hole wall, with rare incidents of instability.

Upon considering the construction technology characteristics, instances of borehole collapse, and the rock and soil mass properties in the formation, it is clear that inappropriate construction technology (including a lack of hole wall protection measures, extended exposure time of the hole wall, excessive drilling depth, and large wall diameter) and poor rock mass properties (including low strength, high in situ stress, susceptibility to disintegration upon water immersion, and high permeability) are the primary and direct causes of borehole collapse. Additionally, engineering experience gained from monopile construction in wind farms indicates that external factors such as fractures, faults, and the operating environment also impact borehole stability to some extent. The causes of borehole instability are summarized and ranked according to their degree of influence, as shown in Figure 14.

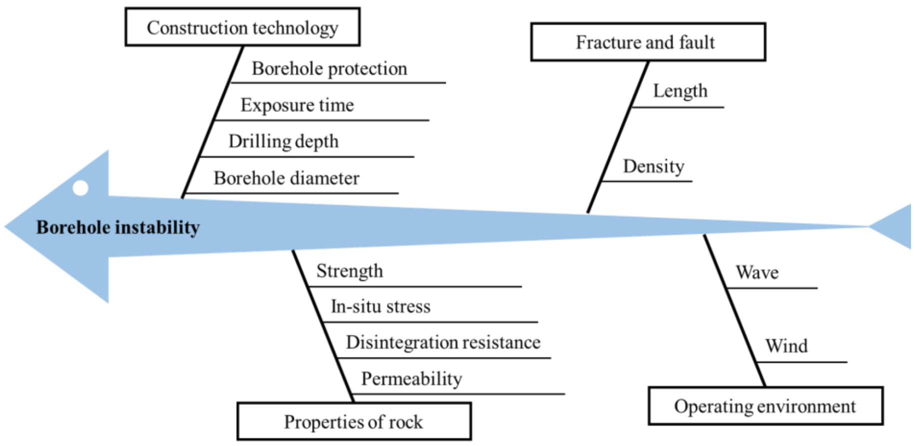

Figure 14. Causes of borehole instability.

(1) The construction of monopiles in this wind farm used the drill-drive-drill method, but the processes between drilling and monopile driving were not rapid enough, resulting in a long-time interval between the two operations. In addition, to shorten the construction time and reduce costs, reverse-circulation drilling with seawater was used during construction instead of using slurry to protect the hole wall, resulting in direct exposure of decomposed granite at the hole wall to water. The long window period between drilling and monopile driving operations and the lack of hole wall protection measures directly led to borehole instability.

Additionally, if the depth of drilling is too large at one time, the increased extent of exposed soil exacerbates the problem of borehole instability. The use of large-diameter monopiles is also an important factor that contributes to borehole instability. The diameter of the monopile is 7 m in the Pinghai Bay offshore wind farm, and the size of the borehole is close to the monopile diameter. The large diameter of the borehole results in a broad range of soil being affected by unloading. Based on the soil arching effect [23], it is evident that the larger the borehole size, the higher the likelihood of hole wall collapse issues.

(2) The insufficient soil shear strength and broken structure of HDG and MDG are the main causes of borehole instability. Drilling and excavation activities change the original in situ stress state of the soil, leading to the loss of horizontal restraint at the hole wall and subsequent changes in the stress state of the soil. The greater the depth of the soil, the higher the original in situ stress and the more pronounced the unloading effect of drilling excavation, exacerbating the change in a stress state. Evidence from the construction of the Pinghai Bay wind farm suggests that collapsed holes tend to occur at depths of 30–40 m, where excavation causes a significant unloading effect on the hole wall. Most of these borehole instabilities occur in MDG and HDG layers, where the shear strength of the soil is not sufficient to resist the shear deformation caused by excavation, resulting in deformation and borehole collapse.

As observed from the three construction cases, the stability of the borehole is influenced by the adjacent strata, but it is fundamentally controlled by the strength of the rock mass. In Case 2, MDG is adjacent to the less weathered and higher strength SDG. According to the previously mentioned stratum variation, the strength of the rock mass increases with depth. As a result, the exposed part of the MDG in this case has a relatively higher strength, leading to a collapse height of only 49% of the original exposed height. In contrast, in Case 3, the exposed rock mass is entirely MDG, and the exposure location has just entered the MDG layer from the HDG layer at 7.3 m. This indicates that the exposed MDG strength is not as high as that in Case 2, which is also reflected in the collapse ratio reaching 98%.

Additionally, CDG and HDG exhibit disintegration properties when immersed in water. Therefore, if the exposed rock after drilling is CDG or HDG, the gradual disintegration due to water immersion can accelerate the collapse of the borehole wall and sustain damage continuously. The duration of soil soaking in water corresponds to the extent of hole collapse. Additionally, the higher the permeability coefficient of HDG, the easier it is for water to seep into the rock, leading to soil mass disintegration and borehole wall collapse.

(3) Geological fractures and faults discovered can aggravate hole wall collapse problems. The MDG formation exhibits many structural planes, which are evident in the block-like nature of the MDG samples collected. These structural planes significantly reduce the overall strength of the rock mass, and the length and density of these planes are crucial factors that affect rock mass strength. Besides, HDG formation also contains geological cracks that, if present in the hole wall, can cause the surrounding rock mass to slide rapidly along these cracks, resulting in a hole wall collapse.

(4) Adverse offshore weather conditions, such as strong winds and large waves, can affect the stability of drilling to some extent. Based on engineering experience, strong winds and large waves make it challenging to maintain vertical drilling during the drilling process, potentially causing slight tilting and increasing the likelihood of borehole instability. Furthermore, dynamic loads from strong winds and large waves can induce small vibrations

in the offshore platform and drilling equipment. These vibrations are transmitted to the hole wall through the drill rod and monopile foundation, exerting a disturbance on the soil and affecting borehole stability. However, although these effects can be detrimental, their impact is relatively small compared to construction technology and rock mass properties.

4.4. Judgement of the Possibility of Borehole Instability

Accurate identification of the type of exposed rock is essential to determine the likelihood of borehole instability during the construction of a rock-socketed monopile in similar formations. This can be achieved through sampling or field tests, such as shear wave velocity testing, and the different types of decomposed granite can be identified by referring to Figure 11, Tables 1 and 2. Based on construction experience at the Pinghai Bay offshore wind farm, for the monopile with a diameter of 7 m, if the exposed rock is of the HDG or MDG, the height of the exposed rock exceeds 4 m, and the monopile installation is not completed within five days after the borehole excavation, serious instability issues are likely to occur in the borehole.

4.5. Improvement Measures to Prevent Borehole Instability

Considering the unfavorable engineering characteristics of decomposed granite, implementing the drive-drill-drive technology for constructing monopiles in multi-layered decomposed granite strata inevitably faces the challenge of borehole instability. However, various measures can be taken to minimize the extent of hole wall collapse and delay its occurrence, mitigating the negative impact on monopile construction. Efforts can be made to drive the monopile foundation deeper into strata with higher soil strength to avoid drilling or to minimize the time interval and drilling depth between drilling and pile driving. Additionally, construction processes can be improved to avoid borehole instability issues, as shown in Figure 15. Specific suggestions for improvement include:

(1) Using a smaller diameter drilling rig during drilling. In this case, the range of exposed soil is reduced, and considering the soil arching effect, the possibility of borehole instability is significantly reduced. Even if borehole instability occurs, the buffer effect provided by the distance between the borehole wall and the monopile can prevent pile running. Additionally, constructing a hollow cylindrical structure of soil within the monopile can also significantly reduce pile driving resistance.

(2) Using a casing that can be lifted and lowered freely. After drilling is completed, the casing can be lowered to protect the borehole wall and then lifted back up after the next step of pile driving is completed. This method can provide support to the borehole wall to prevent borehole instability.

(3) Using biopolymer drilling fluid during drilling to form a filter cake on the borehole wall. This can prevent decomposed granite from directly contacting seawater, avoiding disintegration. It can also exert static water pressure on the borehole wall to counteract the stress release caused by excavation and maintain borehole stability. Compared with traditional slurry, biopolymer drilling fluid causes minimal pollution to the marine environment, but its disadvantage is its high cost.

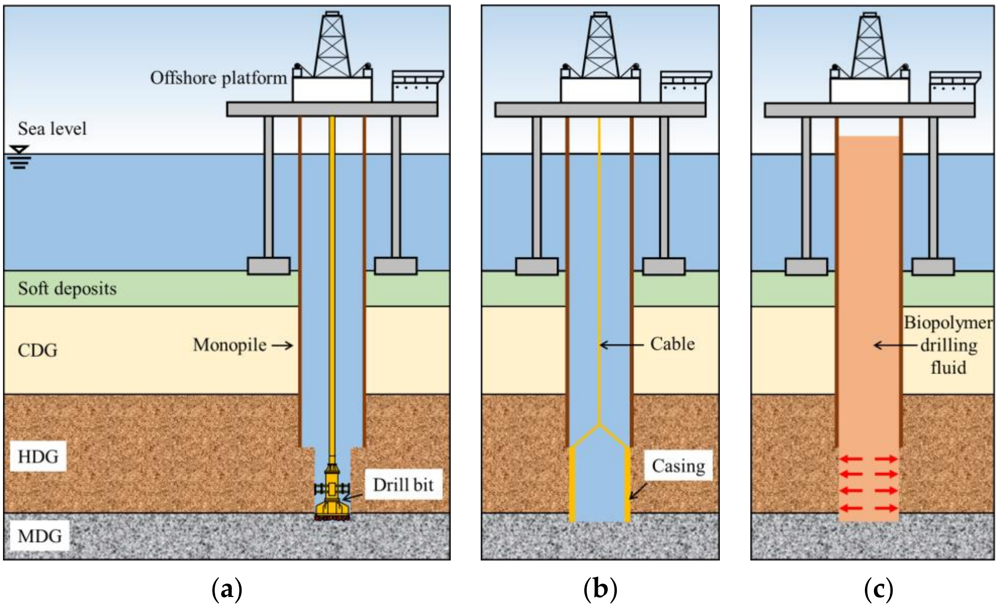

Figure 15. Construction recommendations: (**a**) drilling smaller borehole, (**b**) using casing, and (**c**) using biopolymer drilling fluid.

5. Conclusions

In this research, the causes of borehole instability in the construction of monopiles for offshore wind turbines in Pinghai Bay in decomposed granite seabed were investigated. A series of field sampling, in situ tests, and laboratory tests were conducted to reveal the geotechnical characteristics of marine-decomposed granite in the area. Combining three cases of monopile construction, the reasons for borehole instability during the construction process of rock-socketed monopiles in the decomposed granite seabed were clarified, and corresponding recommendations were proposed. The main conclusions are as follows:

(1) The results of the sampling operation demonstrate that employing a double-tube rotary sampler with biopolymer drilling fluid significantly minimizes disturbance to decomposed granite, enabling the acquisition of complete samples. A series of in situ and laboratory tests revealed an increase in the weathering degree of granite from SDG to MDG, HDG, and CDG, while mechanical strength and integrity declined considerably. These four types of decomposed granite can be effectively classified based on apparent characteristics, in situ tests, and laboratory tests.

(2) The long window period between drilling and monopile driving operations, the insufficient soil shear strength, and the lack of hole wall protection are the main causes of borehole instability. Due to HDG's insufficient strength and the highly fragmented structure of MDG, hole collapse predominantly occurs within CDG and MDG strata. The water-immersion disintegration properties of HDG exacerbate the collapse rate in HDG strata. Additional factors, such as large pile foundation dimensions, geological fractures or faults, and adverse construction environments, may worsen this issue.

(3) The occurrence of hole collapse can be comprehensively determined by considering factors such as stratum type, soil exposure range, and exposure duration. The key to preventing hole wall instability lies in reducing exposed soil range and duration or implementing suitable retaining wall measures. Drilling smaller holes has proven effective in engineering practice. Employing casing or plant-based drilling fluid for hole wall protection may also be considered a potential improvement measure.

Author Contributions: Conceptualization, B.S. and Q.Z.; formal analysis, B.S.; investigation, G.Y. and W.Z.; resources, J.L.; data curation, W.Z. and J.L.; writing—original draft preparation, B.S.; writing—review and editing, Q.Z.; visualization, B.S.; supervision, Q.Z. and G.Y. All authors have read and agreed to the published version of the manuscript.

Funding: This research was funded by National Natural Science Foundation of China (Grant Nos. 42207186, 42072317), the Natural Science Foundation of Shanghai (Grant No. 22ZR1435000), and the Shanghai Pujiang Talent Program (22PJ1408800).

Institutional Review Board Statement: Not applicable.

Informed Consent Statement: Not applicable.

Data Availability Statement: Data is available on request from the authors.

Conflicts of Interest: The authors declare no conflict of interest.

References

1. Global Wind Energy Council. *Global Wind Report 2022*; Global Wind Energy Council: Brussels, Belgium, 2022.
2. Zhang, J.; Wang, H. Development of offshore wind power and foundation technology for offshore wind turbines in China. *Ocean Eng.* **2022**, *266*, 113256. [CrossRef]
3. Gasch, R.; Twele, J. *Wind Power Plants: Fundamentals, Design, Construction and Operation*; Springer Science & Business Media: Berlin/Heidelberg, Germany, 2011.
4. Wu, X.; Hu, Y.; Li, Y.; Yang, J.; Duan, L.; Wang, T.; Adcock, T.; Jiang, Z.; Gao, Z.; Lin, Z. Foundations of offshore wind turbines: A review. *Renew. Sustain. Energy Rev.* **2019**, *104*, 379–393. [CrossRef]
5. Byrne, B.W.; Houlsby, G.T.; Burd, H.J.; Gavin, K.G.; Igoe, D.J.; Jardine, R.J.; Martin, C.M.; McAdam, R.A.; Potts, D.M.; Taborda, D.M. PISA design model for monopiles for offshore wind turbines: Application to a stiff glacial clay till. *Géotechnique* **2020**, *70*, 1030–1047. [CrossRef]
6. Byrne, B.W.; McAdam, R.A.; Burd, H.J.; Beuckelaers, W.J.; Gavin, K.G.; Houlsby, G.T.; Igoe, D.J.; Jardine, R.J.; Martin, C.M.; Muir Wood, A. Monotonic laterally loaded pile testing in a stiff glacial clay till at Cowden. *Géotechnique* **2020**, *70*, 970–985. [CrossRef]
7. Fan, S.; Bienen, B.; Randolph, M.F. Effects of monopile installation on subsequent lateral response in sand. I: Pile installation. *J. Geotech. Geoenviron. Eng.* **2021**, *147*, 04021021. [CrossRef]
8. Chiu, C.; Ng, C.W. Relationships between chemical weathering indices and physical and mechanical properties of decomposed granite. *Eng. Geol.* **2014**, *179*, 76–89. [CrossRef]
9. Liu, X.; Zhang, X.; Kong, L.; Li, X.; Wang, G. Effect of cementation on the small-strain stiffness of granite residual soil. *Soils Found.* **2021**, *61*, 520–532. [CrossRef]
10. Duan, K.; Wu, W.; Kwok, C.Y. Discrete element modelling of stress-induced instability of directional drilling boreholes in anisotropic rock. *Tunn. Undergr. Space Technol.* **2018**, *81*, 55–67. [CrossRef]
11. Fink, J. *Petroleum Engineer's Guide to Oil Field Chemicals and Fluids*; Gulf Professional Publishing: Houston, TX, USA, 2021.
12. Haimson, B. Micromechanisms of borehole instability leading to breakouts in rocks. *Int. J. Rock Mech. Min. Sci.* **2007**, *44*, 157–173. [CrossRef]
13. Lan, H.; Moore, I.D. Experimental investigation examining influence of pump rates on horizontal borehole stability in sand. *Tunn. Undergr. Space Technol.* **2022**, *127*, 104608. [CrossRef]
14. Abdulhadi, N.O.; Germaine, J.T.; Whittle, A.J. Experimental study of wellbore instability in clays. *J. Geotech. Geoenviron. Eng.* **2011**, *137*, 766–776. [CrossRef]
15. Castillo, J.G.; Nagula, S.; Schallück, C.; Grabe, J. Numerical Simulation of Drive-Drill-Drive Techniques for Open-Ended Pile Installations. In *Recent Advancements in Civil Engineering: Select Proceedings of ACE 2020*; Springer: Berlin/Heidelberg, Germany, 2022; pp. 539–548.
16. Li, L.; Ru, D.; Li, K.; Yishan, W. Research and Application of Reverse Circulation Drilling Technology. In Proceedings of the International Oil & Gas Conference and Exhibition in China, Beijing, China, 5–7 December 2006.
17. Viana da Fonseca, A.; Pineda, J. Getting high-quality samples in 'sensitive'soils for advanced laboratory tests. *Innov. Infrastruct. Solut.* **2017**, *2*, 34. [CrossRef]
18. Mayne, P.W.; Christopher, B.R.; DeJong, J. *Manual on Subsurface Investigations*; National Highway Institute Publication No. FHWA NHI-01-031; Federal Highway Administration: Washington, DC, USA, 2001.
19. Xia, S.; Zhang, L.; Davletshin, A.; Li, Z.; You, J.; Tan, S. Application of polysaccharide biopolymer in petroleum recovery. *Polymers* **2020**, *12*, 1860. [CrossRef] [PubMed]
20. *ASTM D2487*; Standard Practice for Classification of Soils for Engineering Purposes. ASTM International (ASTM): West Conshohocken, PA, USA, 2011.
21. Hencher, S.R.; Martin, R.P. The Description and Classification of Weathered Rocks in Hong Kong for Engineering Purposes. In Proceedings of the 7th South-East Asian Geotechnical Conference, Hong Kong, China, 22–26 November 1982; pp. 125–142.

22. Ng, C.W.; Yau, T.L.; Li, J.H.; Tang, W.H. Side resistance of large diameter bored piles socketed into decomposed rocks. *J. Geotech. Geoenviron. Eng.* **2001**, *127*, 642–657. [CrossRef]
23. Li, Z.; Lin, W.; Ye, J.; Chen, Y.; Bian, X.; Gao, F. Soil movement mechanism associated with arching effect in a multi-strutted excavation in soft clay. *Tunn. Undergr. Space Technol.* **2021**, *110*, 103816. [CrossRef]